An experimental study on the drop/interface partial coalescence with surfactants

Teng Dong, Weheliye Hashi Weheliye, Pierre Chausset, and Panagiota Angeli

Citation: Physics of Fluids **29**, 102101 (2017);
View online: https://doi.org/10.1063/1.4985997
View Table of Contents: http://aip.scitation.org/toc/phf/29/10
Published by the American Institute of Physics

Articles you may be interested in

Hydrodynamic interactions between a self-rotation rotator and passive particles
Physics of Fluids **29**, 103301 (2017); 10.1063/1.4997221

Asymptotic growth laws for intrusion tongues in lock-exchange flows
Physics of Fluids **29**, 104101 (2017); 10.1063/1.4994904

The regime of large bubble entrapment during a single drop impact on a liquid pool
Physics of Fluids **29**, 092101 (2017); 10.1063/1.4992124

Dynamics of a single buoyant plume in a FENE-P fluid
Physics of Fluids **29**, 091701 (2017); 10.1063/1.4986749

Interaction of vortex ring with a stratified finite thickness interface
Physics of Fluids **29**, 093602 (2017); 10.1063/1.4994264

When shock is shocked: Riemann problem dynamics at pulse ionization of a shock wave
Physics of Fluids **29**, 101701 (2017); 10.1063/1.4991072

An experimental study on the drop/interface partial coalescence with surfactants

Teng Dong,[1] Weheliye Hashi Weheliye,[1] Pierre Chausset,[2] and Panagiota Angeli[1,a)]
[1]*ThAMeS Multiphase, Department of Chemical Engineering, University College London, London WC1E 6BT, United Kingdom*
[2]*Hydraulics and Fluid Mechanics Department, ENSEEIHT, Toulouse, France*

(Received 30 May 2017; accepted 6 September 2017; published online 2 October 2017)

This paper presents investigations on the partial coalescence of an aqueous drop with an organic-aqueous interface with and without surfactants. The organic phase was different silicone oils and the aqueous phase was a glycerol-water solution at different concentrations. It is found that when the surfactant Span 80 is introduced into the organic phase, the partial coalescence region is reduced in the *Oh–Bo* coalescence map. The range of the inertio-capillary regime reduces when surfactants are present, while the drop size ratio decreases with increasing surfactant concentration. The velocity fields inside the aqueous drop were studied with high speed particle image velocimetry for the first time. In the surfactant-free system, it was found that the inward motion of the fluids at the upper part of the drop favours the generation of a liquid cylinder at the early stages of coalescence. The pressure gradient created by the downward stream at the bottom of the liquid cylinder drives the pinch-off of the secondary drop. When surfactants are present, the rupture of the film between the drop and the interface occurs at an off-axis location. The liquid cylinder formed in this case is not symmetric and does not lead to pinch-off. It is also found that the vortices inside the droplet have little impact on the partial coalescence. © *2017 Author(s). All article content, except where otherwise noted, is licensed under a Creative Commons Attribution (CC BY) license (http://creativecommons.org/licenses/by/4.0/).* https://doi.org/10.1063/1.4985997

I. INTRODUCTION

When a drop approaches the interface of a pool of the same liquid with a layer of another immiscible liquid, it will coalesce with the homophase once the film that initially forms between the drop and the interface ruptures. In many occasions, the drop does not merge completely with the homophase but the top is pinched off and generates a daughter droplet. The process can be repeated many times till the daughter droplet coalesces completely. This phenomenon is called partial coalescence; the dispersed secondary droplets that are produced are important for many meteorological phenomena including cloud drop growth[1,2] and formation of ocean mist carrying salt particles.[3] In industrial applications, the increase of the total coalescence time and the formation of a range of drop sizes caused by partial coalescence decrease the separation efficiency in liquid-liquid coalescers.[4] On the other hand, the small droplets created by partial coalescence can improve the perception of fat-related sensory attributes in the food industry.[5] The range of time and length scales involved in partial coalescence makes the study of the phenomenon challenging and difficult to capture experimentally. Following the first study on partial coalescence by Mahajan,[6] subsequent researchers have managed to describe the whole process and the mechanism. Charles and Mason[7] systematically investigated the partial coalescence of droplets with liquid/liquid interfaces and suggested that it resulted from a Rayleigh-Plateau instability. According to the theory, the daughter droplet is generated through two stages: (1) the volume of the mother drop reduces after the film rupture until it takes the shape of a cylinder; (2) when the height, h, of this liquid cylinder becomes $h > 2r_c$, where r_c is the radius of the cylinder, the top of the cylinder pinches off due to the Rayleigh instability and a daughter drop forms. However, Blanchette and Bigioni[8] found from numerical simulations of drops coalescing with interfaces with air that the pinch-off did not result from the Rayleigh-Plateau instability. To show this, they paused their simulation when the cylinder was fully stretched and restarted it by setting all velocities to zero. This procedure did not lead to pinch-off; it should be noted, however, that the column length h in the simulations did not reach $h > 2r_c$. Instead, Blanchette and Bigioni[8] proposed that the pinch-off was controlled by the competition between the horizontal collapse and vertical collapse of the droplet surface induced by surface tension. From simulations in liquid-liquid systems, Ray, Biswas, and Sharma[9] plotted the u- and v-velocity contours around the drop surface for both the dispersed and the continuous phases and reached the same conclusion. As a result of large differences in properties, the coalescence of a drop with a liquid-liquid interface can be different to that with an air/liquid interface,[10–12] in terms of the boundary between total and partial coalescence, the rest times before the onset of coalescence, and the self-similarity limit for partial coalescence. Consequently, the studies reviewed here only refer to the coalescence of drops with liquid/liquid interfaces unless otherwise indicated. Yue, Zhou, and Feng[13] proposed a theory for partial coalescence based on energy

a)Author to whom correspondence should be addressed: p.angeli@ucl.ac.uk

 © Author(s) 2017

barriers. They found from numerical simulations that the surface area of the drop increased when the neck edges approached each other during pinch-off. The additional interfacial energy associated with the increased drop surface area presented an energy barrier that should be overcome for partial coalescence to occur. Viscous dissipation in the liquids around the interface determined whether the energy barrier could be overcome. Zhang, Li, and Thoroddsen[14] found that during partial coalescence capillary waves carried momentum upwards and at the same time they caused an inward motion of the neck. The upward capillary waves and the drainage rate of the drop liquid were both suppressed in highly viscous systems. They showed, in addition, that pinch-off depended on the geometry of the neck and in particular the relative values of the axial and the azimuthal curvatures.

Apart from the mechanism, other characteristics of partial coalescence, such as drop rest time, coalescence stages, and pinch-off time, have also been investigated. Mar and Mason[15] found that the coalescence of droplets with a liquid/liquid interface had more stages than that with an air/liquid interface. The experimental results of Nikolov, Wasan *et al.*[16] indicated that the stages of partial coalescence were reduced from six to five when surfactant was present. Charles and Mason[7] compared the rest times of the droplets at different coalescence stages. The results showed that the primary drop had the longest rest time, while the rest time for the droplet in the last stage was the shortest. In partial coalescence, the pinch-off time of each stage, which refers to the time interval from the onset of the film rupture to the occurrence of the pinch-off, has been investigated more than the total coalescence time. Zhang, Li, and Thoroddsen[14] found that the pinch-off time for drop-drop coalescence was longer than that for drop-interface coalescence. For drop-drop coalescence, the pinch-off time in the first stage was decreased as the diameter ratio of the two mother droplets increased, while the pinch-off time of the second stage was unaffected. In drop-interface coalescence, the pinch-off time was independent of the drop size in the inertio-capillary regime, but in both the gravity and viscous regimes, it was decreased with increasing droplet size.[17] Yue, Zhou, and Feng[13] plotted the pinch-off time against the average Oh number defined using viscosity equal to $\mu = (\mu_d + \mu_s)/2$ and a specific Oh' defined using $\mu = (3\mu_d + \mu_s)/4$ (as suggested by Kinoshita, Teng, and Masutani).[18] Here, μ_d and μ_s refer to the viscosity of the droplet and the surrounding phase. The results indicated that the viscosity of the droplet had more impact on the pinch-off phenomena than that of the surrounding liquid.

The transition between partial and total coalescence is often plotted in maps with the Oh and Bo numbers as coordinates.[8,17,19] Mohamed-Kassim and Longmire[20] proposed that partial coalescence will occur when $BoOh < 0.02$-0.03, where Oh was defined using the arithmetic average of the viscosities of the two phases. Gilet *et al.*[19] suggested that partial coalescence would take place when $Oh_d + 0.057Oh_s < 0.02$ for $Bo < 0.1$ to account for the influence of the viscosities of both phases.

The ratio of the daughter droplet to mother drop diameter, $\xi = d/D$ (d and D are the diameters of the daughter and the mother drop), is often used to characterise the degree of partial coalescence. Charles and Mason[7] studied experimentally the effect of fluid viscosities on the drop size ratio and found that it varied with the viscosity ratio $\lambda = \mu_d/\mu_s$, where μ_d and μ_s are the viscosities of the drop (aqueous phase) and of the surrounding liquid (organic phase), respectively. There was no partial coalescence when $\lambda < 0.2$ or $\lambda > 11$, while for $\lambda = 1$, the drop ratio reached a maximum value. However, Yue, Zhou, and Feng[13] found numerically that the drop ratio increased with λ increasing from 0.1 to 10. The drop ratio depends also on the coalescence regime. In the inertio-capillary regime, the drop ratio is independent of the drop size, and it decreases as the drop size increases in the gravity regime; it also decreases before reducing rapidly to zero in the viscous regime.[17] The effect of Bo and Oh on the drop ratio ξ was separately analysed by Yue, Zhou, and Feng[13] and was found to be independent of Bo when $Bo < 0.1$. Also, ξ remained constant for $Oh < 0.01$ when Bo was negligible. To predict the drop ratio, Charles and Mason[7] considered the Rayleigh-Plateau instability and assumed that the volume of the daughter droplet is the same to the volume of the liquid cylinder formed in the previous step. The ratio was found to be equal to $\xi = (2Z_0^2/3)^{1/3}$, where Z_0 is a non-dimensional parameter which represents the ratio of the wavelength of disturbance to the diameter of the liquid column.[21] Recently, Kavehpour[22] suggested that $\xi = (1 - 3(Oh + (Oh^2 + 4)^{1/2})/8)^{1/3}$ by fitting a large number of experimental data with good accuracy.

As shown above, partial coalescence has been widely studied. The conditions under which partial coalescence will occur, as well as the approximate size of the drops formed, are well documented for systems without surfactants. Even though in various industrial applications surfactants are present in liquid-liquid systems either naturally or artificially, only a few studies on the partial coalescence with surfactants have been conducted. A number of studies have focused on film thinning and showed that the transport and distribution of the surfactants at the interfaces produce complex phenomena which delay film drainage.[23–26] Blanchette, Messio, and Bush[12] studied the influence of surface tension gradients on the partial coalescence of a droplet with a liquid/air interface and estimated that the surfactants would concentrate at the neck at the early stages of coalescence. The results agreed with recent numerical studies[2,27] which showed that surfactants accumulate at the edges as the neck grows after the film rupture, increasing significantly their concentration locally. Martin and Blanchette[2] found numerically that pinch-off and partial coalescence are inhibited in the presence of surfactants. Their results were validated by Pucci, Harris, and Bush[11] who studied experimentally the partial coalescence of bubbles with soap films when surfactants were present.

The few studies available only report qualitative results on the effect of surfactants on partial coalescence. There is no quantitative information, however, on the changes of the partial coalescence boundary or the ratio of drop sizes when surfactants are added in two-phase systems. In addition, the effects of surfactants on the drop velocity fields during partial coalescence have not been investigated. To address these questions, the current paper investigates the partial coalescence between a drop and a liquid-liquid interface in the presence of surfactants experimentally. High speed shadowgraphy was used to

observe the evolution of the interfaces and the drop size ratios in partial coalescence for a wide range of *Oh* and *Bo* numbers. The velocity profiles and the vorticity structures in the coalescing drops for certain liquid pairs were studied with high speed particle image velocimetry (PIV).

II. EXPERIMENTAL METHODOLOGY

The experimental setup and the techniques used to study partial coalescence of drops with liquid-liquid flat interfaces are described in this section. The experiments were conducted in a transparent acrylic vessel with 5 cm^2 base width and 15 cm height (Fig. 1). The bottom of the vessel was filled with the aqueous phase, and the organic phase was added on top, forming a liquid/liquid interface. The aqueous droplets were generated through stainless steel nozzles located at 1 cm above the interface. The sizes of the droplets were varied by using nozzles with different internal diameters equal to 0.5 mm, 1 mm, and 2 mm. The nozzles were connected to a syringe mounted on an Aladdin® syringe pump that was operated at a constant flow rate of 0.2 ml/min. Two techniques, shadowgraphy and particle image velocimetry, were used to study the evolution of partial coalescence and of the flow fields inside the coalescing drops, and these are described in detail below.

A. Setup for shadowgraphy measurements

In shadowgraphy, the observation area was lit by a backlight located behind the vessel, as shown in Fig. 1. The images of drop coalescence were captured by a high-speed camera set in front of the vessel, which was equipped with a mono-zoom Nikon lens giving a field of view of 9×9 mm^2. The camera was inclined downwards to view the drop bottom. As the aim of the shadowgraph experiments was to investigate whether the coalescence was partial or total and the drop diameter ratio at each coalescence stage, a low frame rate of 1000 fps was used for the high-speed camera. Typical shadowgraphy images that show the cascade of partial coalescence are presented in Fig. 2(a).

Experiments were carried out both without and with surfactants. The organic phase was 5 cSt silicone oil and the aqueous phase was a glycerol-water solution with different

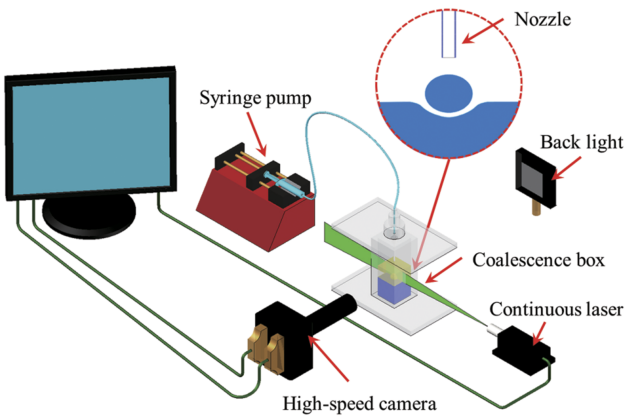

FIG. 1. Schematic of the experimental setup for the coalescence experiments.

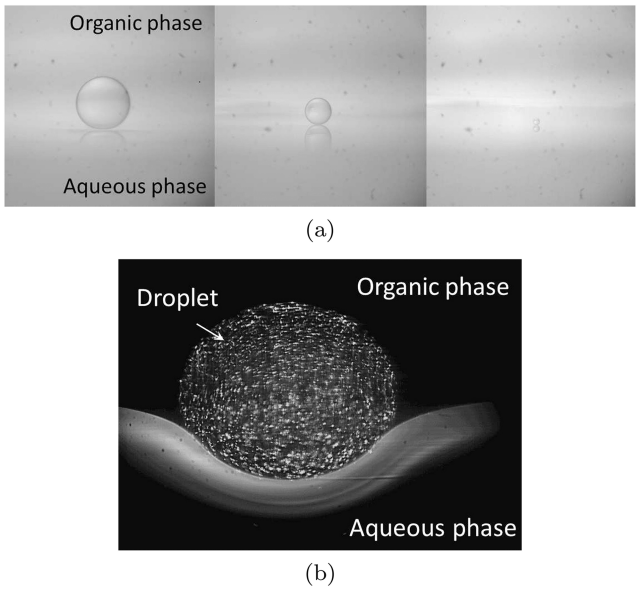

FIG. 2. Raw images obtained from (a) shadowgraph and (b) PIV.

volume concentrations, ζ. For the experiments with surfactants, oil soluble Span 80 was added in the oil at mass ratios, φ, of surfactant to oil equal to 0, 2×10^{-5}, 5×10^{-5}, 1×10^{-4}, and 2×10^{-4}. Span 80 (HLB = 4.3, Mw = 428.61 g/mol) is a non-ionic surfactant that is commonly used in the formulation of stable emulsions. A detailed description of the properties of Span 80 under similar conditions can be found elsewhere[28] and are only briefly summarized here. The properties of the liquids are shown in Table I, where SO refers to silicone oil and S80 refers to Span 80. The interfacial tension under each concentration was measured with the Du Nouy ring method.

B. Setup for PIV measurements

The velocity fields inside the drops during partial coalescence were studied with Particle Image Velocimetry (PIV). The PIV setup was similar to that of the shadowgraphy. The difference was that the backlight was removed and the observation area was illuminated by a Laserglow® continuous diode laser (300 mW) with a wavelength of 532 nm and 4 mm beam size (Fig. 1). A cylindrical lens was mounted in front of the laser creating a laser sheet of approximately 1 mm thickness. To remove optical distortion and improve the quality of the PIV images close to the interface, the refractive indices of the organic and the aqueous phases were matched. The results from the shadowgraphy experiments showed that 0.65 cSt silicone oil and a water-glycerol mixture gave partial coalescence. It was found that 33% of glycerol in water ($r_{wat:gly}$ = 1.372 at room temperature) matched the refractive index of the 0.65 cst silicone oil ($r_{0.65cst}$ = 1.372, 20 °C) within 0.01%. The refractive indices were measured with an Abbe 5 refractometer (BS).

For the PIV experiments, the initial mother droplet was seeded with 1 μm Rhodamine coated particles. Since the two phases have a matching refractive index, the interface cannot be seen in the images and a thin layer of Rhodamine 6G was added at the interface to make it visible. Measurements

TABLE I. Fluid properties.

	Fluids						
	Aqueous phase	Organic phase	ρ_d (kg/m^3)	ρ_s (kg/m^3)	μ_d (mPa s)	μ_s (mPa s)	σ (mN/m)
Shadowgraph observation	100%W	5 cSt silicone oil	1000	914	1.00	4.57	39.7
	75%W + 25%G		1059		1.97		32.3
	65%W + 35%G		1085		2.85		30.7
	57.5%W + 42.5%G		1105		3.99		30.0
	100%W	5SO + 2×10^{-5} S80	1000	914	1.00	4.57	33.8
		5SO + 5×10^{-5} S80					26.7
		5SO + 1×10^{-4} S80					21.4
		5SO + 2×10^{-4} S80					15.5
	75%W + 25%G	5SO + 2×10^{-5} S80	1059	914	1.97	4.57	27.8
		5SO + 5×10^{-5} S80					24.2
		5SO + 1×10^{-4} S80					19.2
PIV tests	67%W + 33%G	0.65 cSt silicone oil	1080	761	2.599	0.49	20.20
		0.65SO + 1.3×10^{-6} S80					11.88
		0.65SO + 1.3×10^{-4} S80					1.97

showed that the presence of Rhodamine 6G or the tracer particles in the aqueous phase did not affect the interfacial tension values and the drop ratio, ξ (variation of less than 5% for both cases). A typical PIV raw image of a drop immersed in a pool of liquid is shown in Fig. 2(b). For these experiments, two surfactant concentrations, $\varphi = 1.3 \times 10^{-6}$ and $\varphi = 1.3 \times 10^{-4}$, were used. The frame rate of the high-speed camera was set at 5400 fps for all the PIV studies. Each set of experiments was repeated over 20 times. After each experiment, the tracer particles in the bulk liquid, which were mainly found close to the interface, were removed with a suction pump to avoid their accumulation in this region. The images obtained from the camera were treated by the open source freeware JPIV where an adaptive correlation tracking of the full image was applied with a final interrogation window of 32×32 pixels. A 50% window overlap was used for a final resolution of 16×16 pixels, corresponding to an area of 0.14×0.14 mm^2.

To check the repeatability of the PIV results, the average circulation level,[29–31] Γ_ω, inside a coalescing droplet, over 10 tests, was plotted for $\varphi = 0$ and $\varphi = 1.3 \times 10^{-6}$. The circulation, Γ_ω, was estimated from Eq. (1) where the integral was carried out over the area, A_ω, which corresponds to a vorticity level $\omega_z > 10$ s^{-1},

$$\Gamma_\omega = \frac{\int_{A_\omega} |\omega_z| \, dA_\omega}{A_\omega}. \quad (1)$$

The film rupture point is close to the central axis when there is no surfactant, while it is away from the centre in the presence of surfactants; in the latter case, the two vortices generated at the bottom of the droplet after the film rupture might travel over different path lengths. As the evolution of circulation levels Γ_ω depends on the paths that the vortices follow, the vortices along the longer paths were considered. As shown in Fig. 3, Γ_ω for different coalescence events under the same conditions evolve in a similar trajectory. The errors in Γ_ω are acceptable except for few points in the high surfactant concentration. A large number of runs were carried out for a given case and relative errors below 15% were considered acceptable.

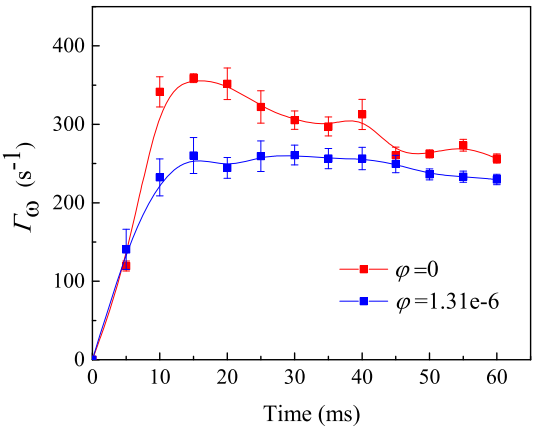

FIG. 3. Variation of circulation level Γ_ω against coalescence time.

III. RESULTS AND DISCUSSIONS

A. Boundary between partial and total coalescence

The partial coalescence involves 7 independent parameters, namely, the viscosities of the aqueous and the organic phases, μ_d and μ_s, respectively, the densities of the aqueous and the organic phases, ρ_d and ρ_s, respectively, the diameter of the mother droplet D, the interfacial tension σ, and the gravitational acceleration g. Four dimensionless groups are thus formed, the Bond number $Bo = \rho g D^2/\sigma$, the Ohnesorge number $Oh = \mu/\sqrt{\rho\sigma D}$, the viscosity ratio $\lambda = \mu_d/\mu_s$, and the density ratio $\eta = \rho_d/\rho_s$.

To account for both gravity and buoyancy, the Bond number is written as $Bo = \Delta\rho g D^2/\sigma$, where $\Delta\rho$ is the density difference between the aqueous and the organic phases and D is the initial horizontal diameter of the mother drop. The

occurrence of partial coalescence is closely related to the pinch-off phenomenon at the upper part of the drop, which depends on the competition between the liquid draining from the drop to the homophase and the speed that the neck contracts at pinch-off. When *Bo* is large, gravity dominates the coalescence process and the drop liquid drains much faster than the contracting speed of the neck. As a result, the drop ratio ξ is monotonically decreasing with *Bo*, and a critical Bond number Bo_c exists above which there is no partial coalescence.[19] When *Bo* is small, mainly the viscous forces resist the surface tension forces and the *Oh* number is used instead to describe partial coalescence. For large *Oh*, the viscosity forces become significant and dampen the capillary waves thus allowing more time for the liquid in the drop to drain out before pinch-off generates a secondary drop.[17,32] Above a critical Oh_c number, there is no partial coalescence. In the literature, there is no general consensus on whether the viscosity of the drop or of the surrounding liquid is more important for partial coalescence and different forms of the *Oh* number have been suggested. Investigators have used the higher of the two viscosities,[22] or the viscosity of the drop phase only,[8,13,17] to calculate the *Oh* number, or have considered more than one *Oh* numbers based on the drop liquid Oh_d and on the surrounding liquid Oh_s.[9,19] According to Kinoshita, Teng, and Masutani,[18] the viscosity of the droplet is more important in partial coalescence, and this will be used subsequently for the estimation of the *Oh* number. In addition, the density is taken equal to the arithmetic mean of the densities of the two phases, $\rho_m = (\rho_d + \rho_s)/2$. The *Oh* number is then calculated as follows: $Oh = \mu_d/\sqrt{\rho_m \sigma D}$. Based on the above, a coalescence map with the boundary between partial and total coalescence is plotted with *Bo* and *Oh* as coordinates.

The coalescence map for the non-surfactant systems is shown in Fig. 4. The values of the *Bo* and the *Oh* numbers were changed by varying the glycerol concentration ζ in water (0%, 25%, 35%, and 42.5%) and the size of the mother drops. As shown in Fig. 4, there exists a critical Oh_c number when *Bo* < 1, which increases slightly as the glycerol concentration increases from 0% to 35%. A similar increase was also observed by Chen, Mandre, and Feng.[17] According to Yue, Zhou, and Feng[13] and Zhang *et al.*,[33] increasing the viscosity of the liquid in the drop delays its drainage and favours partial coalescence. For ζ > 35%, where the corresponding *Bo* number is large, the effect of viscosity is diminished and the Oh_c number does not continue to increase.

The Oh_c number in the current experiments increases from 0.01 to 0.02, while it increased from 0.02 to 0.03 in the experiment by Chen, Mandre, and Feng[17] for similar aqueous phases. In the experiments by Chen, Mandre, and Feng,[17] the organic surrounding phase was decane with 1 mPa s viscosity, which is about 1/5 of the viscosity of the silicone oil in this work. As the viscosity of the surrounding liquid increases, the contracting speed of the neck is inhibited and the transition to total coalescence happens at a reduced droplet based Oh_c. The effect of the viscosity ratio $\lambda = \mu_d/\mu_s$ on the critical Oh_c number was discussed by Yue, Zhou, and Feng.[13] The results show that the critical Oh_c number increases linearly with the viscosity ratio when *Bo* is very small. For $0.22 < \lambda < 0.88$, which is the range of the current experiments, Oh_c increases from 0.01 to 0.02. When λ varies from 1 to 3.4, as in the experiments by Chen, Mandre, and Feng,[17] the Oh_c number is larger and varies from 0.02 to 0.03.

Figure 5 shows the partial and total coalescence regions when surfactant is introduced into the oil at concentrations varying from $\varphi = 2 \times 10^{-5}$ w/w to $\varphi = 2 \times 10^{-4}$ w/w. As can be seen, the partial coalescence region is largely reduced when surfactant is present. According to Martin and Blanchette,[2] the decrease of critical Oh_c can be attributed to the uneven distribution of surfactants along the interface. Just after the film breakage, the edges of the meniscus between the drop and the bulk homophase retract outwards rapidly, with speed higher than the rate of surfactant redistribution at the interface.[34] Therefore, the surfactant accumulates at the neck. Initially

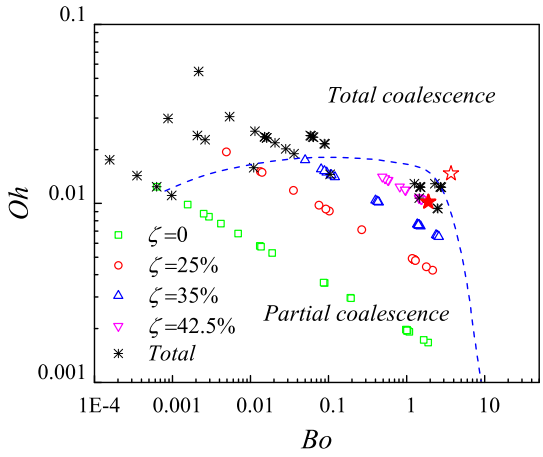

FIG. 4. *Oh–Bo* map for coalescence in surfactant-free systems. The open symbols represent the partial coalescence data with glycerol concentrations in the aqueous phase ranging from ζ = 0% to ζ = 42.5%, the asterisks show the total coalescence data for all glycerol concentrations. The stars refer to the conditions investigated with PIV. The dashed line is for reference only and shows the boundary between the partial and total coalescence regions.

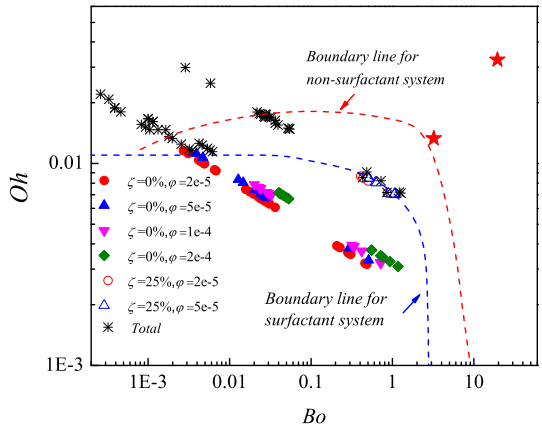

FIG. 5. *Oh–Bo* map for coalescence in surfactant-laden systems. The closed symbols represent the partial coalescence data with different surfactant concentrations for ζ = 0%, the open symbols represent the partial coalescence data with different surfactant concentrations for ζ = 25%. The asterisks show the total coalescence data for all cases. The stars refer to the conditions investigated with PIV. The dashed lines are only for reference and show the boundary between the partial and the total coalescence regions for both surfactant-free and surfactant-laden systems.

capillary waves move upwards to the top of the drop. The top surface is stretched by the momentum of the capillary waves while the increase in area decreases the local concentration of the surfactants in this region. As a result, a surface tension gradient builds between the top and the bottom of the drop, which creates large tangential forces that promote the contraction of the interface and drive the liquid out of the drop. The surfactant concentration remains high locally at the neck, even at the later stages which resists the contraction of the neck edges and the pinch-off. In addition, the sharp curvature at the neck creates a large Laplace pressure that also resists pinch-off. The combined action of the two effects prevents pinch-off and partial coalescence.

It was also observed that for pure water, the critical Oh_c number for the partial coalescence slightly decreases when the surfactant concentration increases from $\varphi = 0$ to $\varphi = 2 \times 10^{-4}$. While for the glycerol solution with $\zeta = 25\%$, the critical Oh_c number reduces significantly even with a small amount of surfactant. The trend agrees well with the numerical data of Martin and Blanchette[2] which reveal that the critical Oh_c number decreases fast with the addition of surfactant for highly viscous drop liquids. An increased viscosity not only dampens the motion of the capillary waves but also resists the movement of the surfactant molecules along the interface and favours total coalescence. For pure water, it is relatively easy for the surfactant molecules to relocate along the interface. In the 25% glycerol solution, which has viscosity two times larger than that of pure water, it is more difficult for the surfactant molecules to spread.

B. The effect of surfactants on the drop ratio

In this section, the effect of the surfactants on the drop size ratio ξ is analysed. Thoroddsen and Takehara[32] identified a narrow regime for a drop coalescing with an air-liquid interface where both the viscous and gravitational forces are negligible and a constant drop ratio $\xi \approx 0.5$ is found for all steps of partial coalescence. Chen, Mandre, and Feng[17] stated that partial coalescence can be extended to all three regimes, i.e., the gravity, the inertio-capillary regime, and the viscous regime. The drop ratio in each regime is plotted for different surfactant concentrations in Fig. 6, with the data taken from all

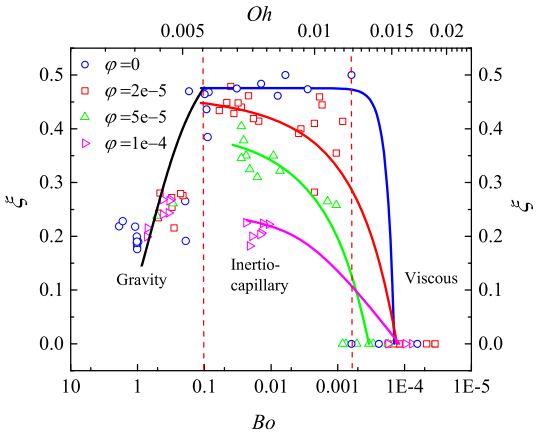

FIG. 6. Daughter to mother drop size ratio in different regimes for the systems with surfactants.

stages of the partial coalescence cascade. The solid lines are drawn to show the trends in the drop ratio at different concentrations. The drop size ratio data were plotted in the gravity regime against the *Bo* number, which indicates the relative importance of the gravitational and the surface tension forces while in both the inertio-capillary and the viscous regimes it was plotted against the *Oh* number. As discussed by Chen, Mandre, and Feng,[17] $Bo = 0.1$ can be taken as the boundary between the gravity and the inertio-capillary regimes. In the gravity regime, the drop ratio for all the surfactant concentrations studied, $\varphi = 0$, $\varphi = 2 \times 10^{-5}$, $\varphi = 5 \times 10^{-5}$, and $\varphi = 1 \times 10^{-4}$, does not change significantly. This is expected since the addition of the surfactants only slightly affects the density of the aqueous phase which is important in this regime. Chen, Mandre, and Feng[17] also found that in this regime, the drop ratios were around 0.25 for $Bo \approx 1$. The variations in ξ are attributed to daughter drops that may form displaced from the focus plane.

Conversely, the presence of surfactants has a great effect on the drop size ratio in the inertio-capillary and the viscous regimes. For $\varphi = 0$, the drop size ratio at each coalescence stage is almost constant and around 0.5 in the inertio-capillary regime between $Oh \approx 0.005$ and $Oh \approx 0.012$. The drop size ratio decreases rapidly to zero when *Oh* increases further. This trend is in agreement with the results by Chen, Mandre, and Feng[17] and the boundary between the inertio-capillary and the viscous regimes is set at $Oh = 0.01$ for the non-surfactant system (see Fig. 6). When surfactants are present, the drop size ratio in the inertio-capillary regime decreases. For $\varphi = 2 \times 10^{-5}$ and $\varphi = 5 \times 10^{-5}$, the value of ξ decreases to around 0.45 and 0.35, respectively, at the boundary with the gravity regime, while for $\varphi = 1 \times 10^{-4}$, the ratio becomes as low as ~0.22, which is less than half of the value for $\varphi = 0$. Surfactants also reduce the range of *Oh* for the inertio-capillary regime, while the transition to the viscous regime becomes less clear. This is attributed to the decrease of the interfacial tension caused by the surfactants. Interestingly, in the presence of surfactants, in the inertia-capillary regime the drop ratio does not remain constant any more but decreases with increasing *Oh*. It should be noted that when surfactants are present, the drop ratio is not constant in each step of a partial coalescence sequence. According to Martin and Blanchette,[2] the concentration of surfactants along the surface of the daughter droplet is higher than that of the previous mother drop. Therefore, the drop ratio will decrease in every coalescence step, as a result of the corresponding lower interfacial tension. However, the distribution of the surfactants along the surface of the droplets in every stage needs to be confirmed experimentally.

C. Evolution of the drop surface during coalescence

The effects of surfactants on the evolution of the drop surface in both partial and total coalescence are analysed in this section. The raw PIV images for indicative partial, boundary, and total coalescence cases are present in Fig. 7. From these images, the drop surface profiles at different time steps under each condition were extracted manually by detecting the boundary between the particle area and non-particle area and are shown in Fig. 8. The continuous blue lines at the upper

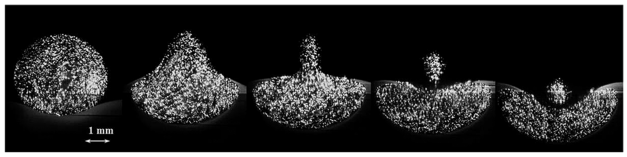

(a)Partial coalescence, φ=0

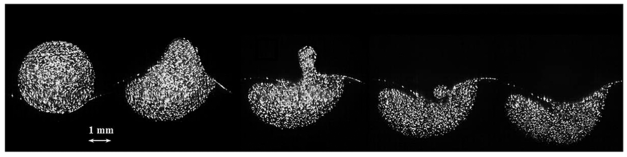

(b)Boundary coalescence,φ=1.3×10^{-6}

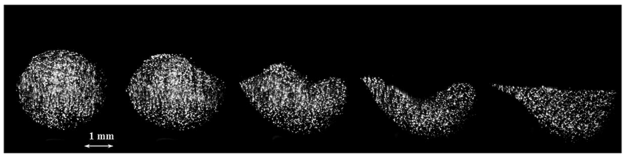

(c)Total coalescence,φ=1.3×10^{-4}

FIG. 7. Enhanced raw PIV images obtained for (a) partial, (b) boundary, and (c) total coalescence.

part of the drop indicate the real drop surface, while the dashed red lines at the bottom part distinguish the fluid with particles, originating from the drop, from the bulk liquid at the lower part of the tank. In Fig. 8, the profile of the drop and the dashed line were plotted in the plane of x–y, and then the figures at different time steps were allocated along the t axis. The time interval is scaled with the capillary time $t_\sigma = (\rho_m R^3/\sigma)^{1/2}$. Here, R refers to the radius of the drop. In Fig. 8(a), the shape evolution is shown for partial coalescence with 0.65 cst silicone oil and 33% glycerol/water mixture. The droplet has horizontal diameter equal to D = 3.33 mm. It can be observed that the droplet rests at the interface and deforms it significantly prior to the film rupture. Once rupture occurs, the sudden retraction of the film creates capillary waves at the bottom of the droplet. At the initial stages, the capillary waves are clearly observed climbing upwards the drop surface. In a short time, the waves reach the summit of the drop where they converge and distort it. From $t = 0.1$ to $t = 0.95t_\sigma$, the drop top surface is squeezed upwards, which causes a small amount of liquid to rise higher than the level of the initial top of the drop. Blanchette and Bigioni[8] found that in air-water systems, the liquid could rise above the initial drop top level by as high as 30% of the initial drop diameter. In the current experiments, the rise was about 4%–10% of the initial drop diameter. The viscosity of the surrounding organic phase seems to reduce this increase in drop height. After about $t = 0.95t_\sigma$, the height of the top of the drop starts to decrease, while the sides of the drop move inwards until a cylinder is formed at $t = 1.13t_\sigma$. The height to diameter ratio of the cylinder for all experiments was found to be much smaller than π, which means that the Raleigh-Plateau instability is not activated.[7] After $t = 1.13t_\sigma$, the bottom part of the liquid cylinder continues to contract and is finally pinched off at $t = 1.37t_\sigma$. The liquid cylinder breaks away and a daughter droplet is formed. As the surface curvature at the bottom of the daughter droplet is much higher than at the top, the droplet tends to recover its spherical shape because of the Laplace pressure. This reduces the downward speed of the droplet,

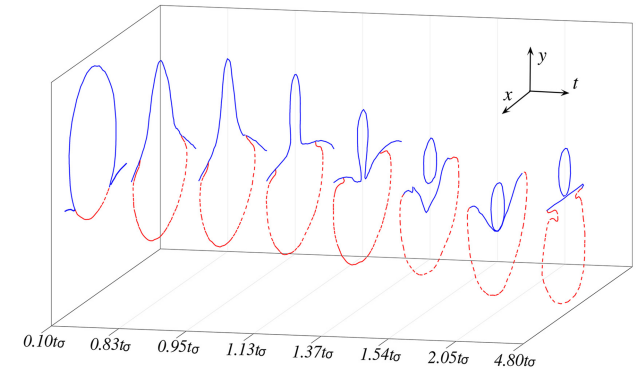

(a)Complete pinch-off,φ=0

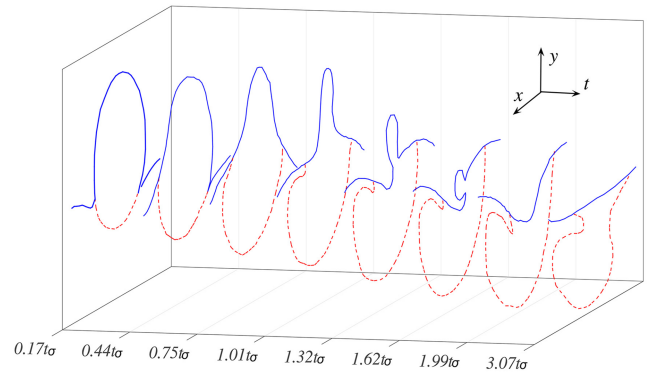

(b)Failed pinch-off,φ=1.3×10^{-6}

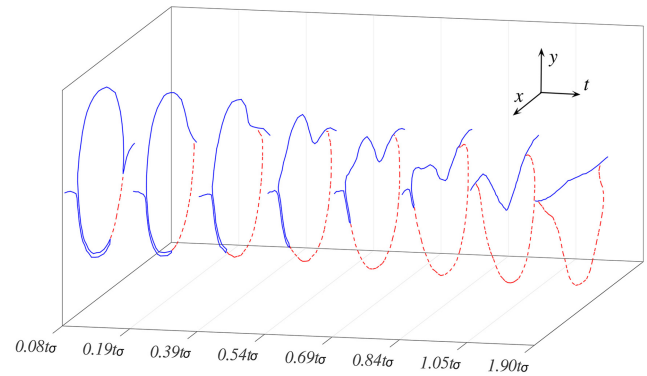

(c)Total coalescence,φ=1.3×10^{-4}

FIG. 8. Drop surface evolution for (a) partial, (b) boundary, and (c) total coalescence. The visualization of the drop surface is stereoscopic. The drop profile at each time step is plotted in the x–y plane first, and then the figures are presented along the t axis.

which becomes less than that of the interface. The bulk interface under the inertia of the draining drop moves downwards and reaches a minimum height at $t = 1.54t_\sigma$. Accordingly, the separation between the droplet and the interface increases between $t = 1.37t_\sigma$ and $t = 1.54t_\sigma$. Once the droplet becomes almost spherical, it starts moving downwards and contacts the rising interface at $t = 2.05t_\sigma$. The droplet and the interface finally move to the quiescent level at $t = 4.80t_\sigma$.

The droplet surface evolutions for the same fluids and two different surfactant concentrations are shown in Figs. 8(b)

and 8(c) for $\varphi = 1.3 \times 10^{-6}$ and $\varphi = 1.3 \times 10^{-4}$, respectively. The corresponding drop sizes are $D = 3.29$ mm and $D = 2.99$ mm. It is clearly observed that the initial deformation of the interface is increased with the surfactant concentration. The increase of the surfactant concentration also shifts the rupture points off-axis.[29] For $\varphi = 0$, the rupture points are close to the center axis of the drop and the average horizontal distance between the rupture point and the central axis over 15 coalescence events is $(0.24 \pm 0.06)D$. This distance increases to $(0.36 \pm 0.03)D$ for $\varphi = 1.3 \times 10^{-6}$. At the low surfactant concentration at $t = 0.44t_\sigma$, the oil film takes longer to retract outwards on the right-hand side of the rupture point, while on the left-hand side, the film drainage has already finished. A cylinder is again formed from the shrinking coalescing drop but the left bottom side of the cylinder is much lower than the right one as shown at $t = 1.32t_\sigma$. Under the inertia of the liquids, the left edge of the neck continues to move downwards to the right, while the right edge of the neck is dragged upwards by the Laplace force. Thus the cylinder is leaning to the left and continues to reduce in size until the interface becomes smooth under the action of surface tension at $1.99t_\sigma$. Pinch-off in this case has failed. This type of coalescence was assigned at the boundary between coalescence regimes. When the surfactant concentration increases to $\varphi = 1.3 \times 10^{-4}$, the interface deforms significantly and nearly half of the drop is under the initial flat interface height. On this occasion, the rupture occurs close to the periphery of the drop, even further away from the on-axis location than for $\varphi = 1.3 \times 10^{-6}$. At $t = 0.08t_\sigma$, the film has already drained on the right while on the left there is still film with a large curvature. The left edge of the neck reaches the flat interface at $t = 1.05t_\sigma$ while most of the liquid in the drop has already mixed with the bulk homophase. In this case, no cylinder is formed. The drop surface approaches the final flat interface position for total coalescence, which is similar to previous observations by Mohamed-Kassim and Longmire[20] and Weheliye, Dong, and Angeli.[29]

D. Velocity fields inside the droplet during coalescence

In this section, the 2D time-resolved velocity fields inside the droplet during partial coalescence as well as in the boundary case are discussed. The results presented here are from a single case unless otherwise stated. Indicative results are shown in Fig. 9, with the vertical velocity (v-velocity) fields in the left column and the horizontal velocity (u-velocity) fields in the right column. The solid line in each figure shows the interface of the bulk and of the drop, while the dashed line shows the area with tracer particles after the film rupture. The time steps are similar to those plotted in Fig. 8. The velocity field evolution for partial coalescence without surfactant is presented in Fig. 9. In the beginning ($t = 0.10t_\sigma$), the top part of the drop is not moving and only the liquid at the bottom starts to flow downwards with a relatively low speed. At the same time, an outflow of the liquid near the bottom interface is generated by the retracting thin film (along the dashed line). In the area near the interface just above the neck, the curved drop surface induces a Laplace pressure that pushes the liquid inwards. Thus, a pair of horizontal velocity components with opposite directions forms near the neck (region A). Similar horizontal velocity pairs

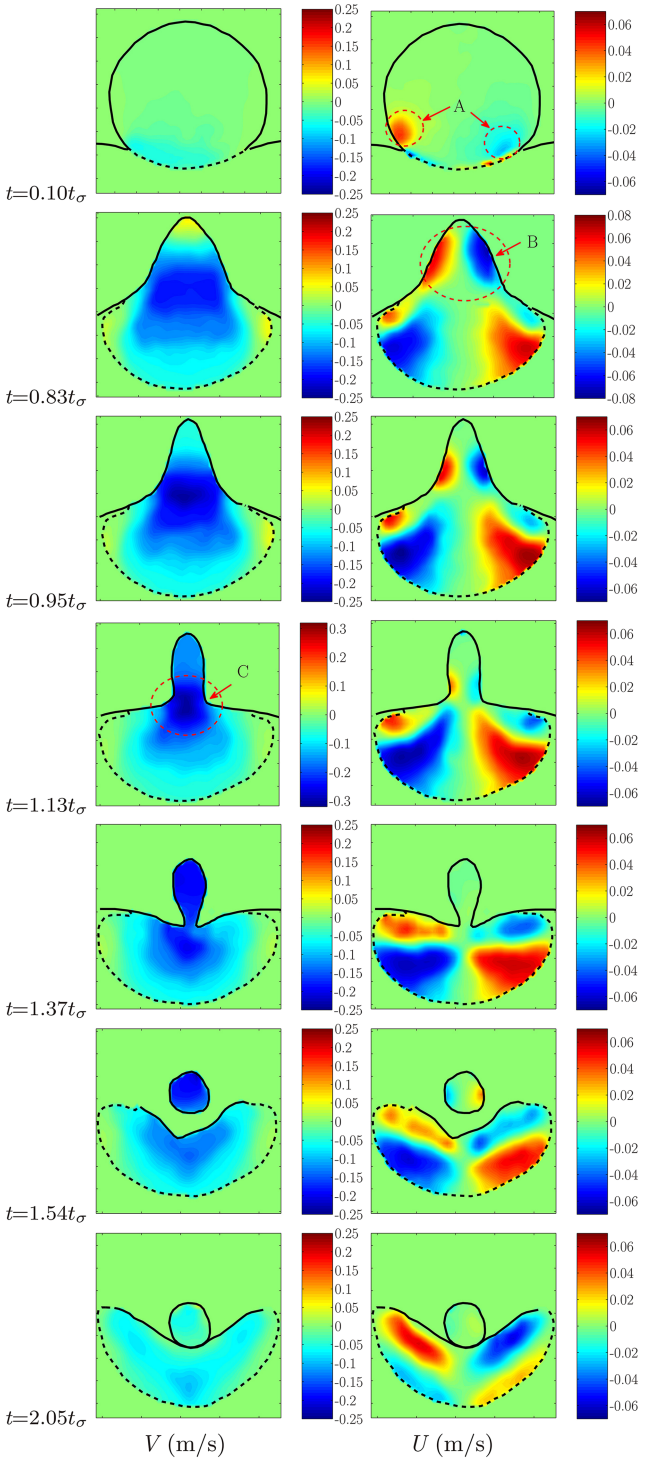

FIG. 9. The vertical and horizontal velocity profiles inside the droplet at different time steps for $\varphi = 0$.

were also observed in the numerical simulations by Blanchette and Bigioni[8] of a drop coalescing with an air/liquid interface. They reported that the velocity pairs were coupled with the upward capillary waves on the drop upper surface. However, this is not seen here, probably because the interfacial capillary waves are suppressed by the viscosity of the surrounding liquid.

At $t = 0.83t_\sigma$, the u-velocity (right column) contour plot shows a large area of the liquid which approaches the middle

of the drop with an average velocity of around 0.04 m/s (region B). Meanwhile, in the middle of the drop, there is also a large area of gravity-driven downstream flow (v-velocity). At $t = 0.95t_\sigma$, the inward horizontal velocities cause the liquid column to shrink. At longer times, $t = 0.95t_\sigma$-$1.37t_\sigma$, the radius of the neck decreases and the outward Laplace forces increase which resist the pinch-off; as a result the u-velocities decrease. However, the edges of the neck continue to approach driven by the inertia of the liquid. When the liquid cylinder is formed at $t = 1.13t_\sigma$, the fluid at the bottom of the cylinder has higher v-velocity and accordingly lower pressure compared to the surrounding area (region C). This low-pressure area has also been reported in the numerical studies by Ding *et al.*[35] and Martin and Blanchette.[2] The reduced pressure drives the edges of the neck to contact with each other and causes the pinch-off at $t = 1.37t_\sigma$.

When surfactant is present at $\varphi = 1.3 \times 10^{-6}$, the film drainage is not symmetrical and the film rupture occurs at an off-axis location (Fig. 10). The liquid at the bottom of the drop has a distinct u-velocity at $t = 0.17t_\sigma$-$0.44t_\sigma$. At the left side, the retracting film carries the fluid outwards and causes the collapse of the drop left surface. At $t = 0.17t_\sigma$, the liquid near the left surface has a small velocity towards the right driven by the collapsing surface (region D); a similar velocity is not observed at the right side. At a later stage ($t = 0.44t_\sigma$), most of the liquid inside the drop starts to move downwards. However, the average v-velocity is about 0.05 m/s, which is much lower than that at $\varphi = 0$ (0.15 m/s). The drop surface on the right-hand side also begins to collapse, and the liquid near the upper right surface starts to move towards the left driven by the collapsing surface. At $t = 0.44t_\sigma$, the horizontal negative streams from the top-right and the bottom-left parts of the drop join and occupy a large area. Because of the flow asymmetry, at $t = 0.75t_\sigma$, the horizontal velocity on the right side has a high value and occupies a large area, which drives the interface on the right to a concave shape while the left is flat (region E). Similar to the case of $\varphi = 0$, the downward stream at the bottom of the liquid cylinder reduces the pressure at this region and helps the pinch-off of the interface at $t = 1.01t_\sigma$. As the velocity difference for $\varphi = 1.3 \times 10^{-6}$ is lower compared to $\varphi = 0$, the corresponding pressure gradient that drives the pinch-off is less. In addition, the flow asymmetry makes the liquid cylinder inclined to the left when the pinch-off is about to happen which increases the local curvature of the interface ($t = 1.62t_\sigma$). As Zhang, Li, and Thoroddsen[14] discussed, the pinch-off is prevented because of the local large curvature of the neck. The interface finally becomes flat under the effect of the Laplace force and no secondary drop forms. When the surfactant concentration increases to $\varphi = 1.3 \times 10^{-4}$, a typical total coalescence is observed which was discussed previously.[29]

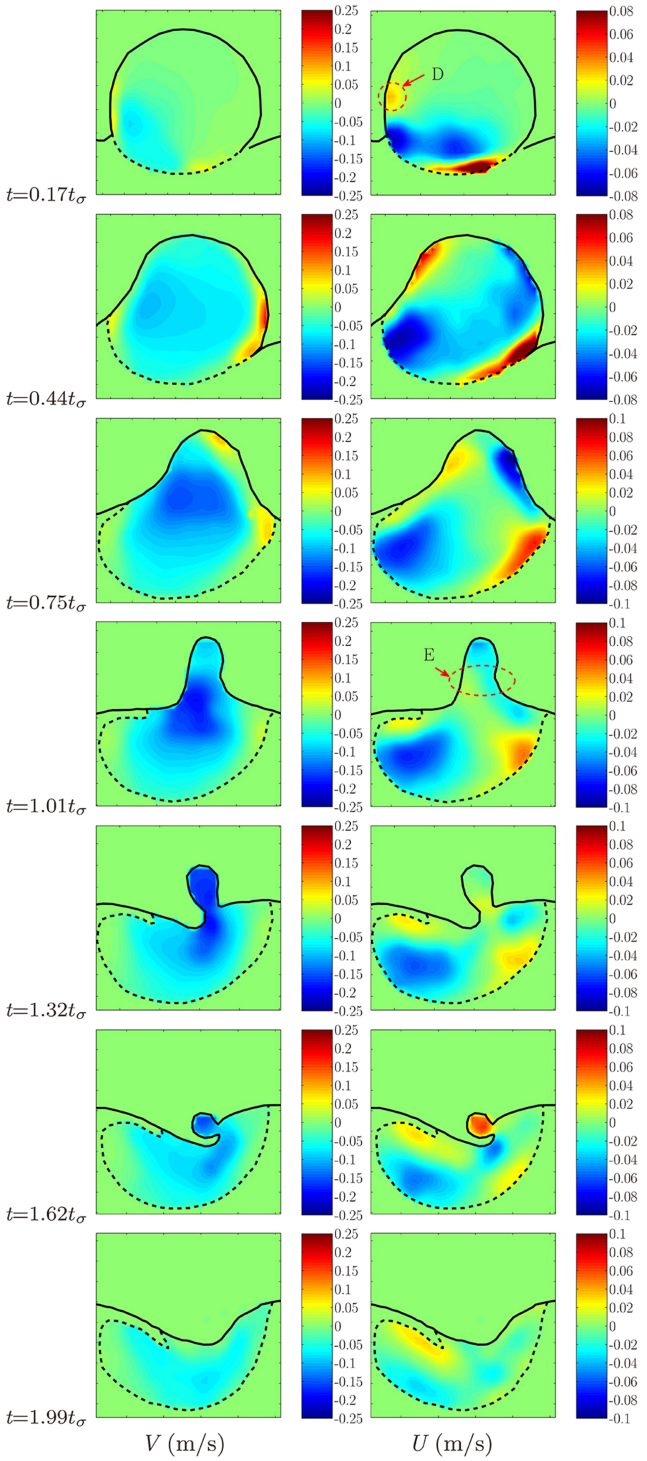

FIG. 10. The vertical and horizontal velocity profiles inside the droplet at different time steps for $\varphi = 1.3 \times 10^{-6}$.

E. Vorticity fields inside the droplet during coalescence

As reported for total coalescence,[20,29] two counter-rotating vortices are created near the bottom of the droplet just after the film breaks up, which then expand inside the droplet during coalescence. In partial coalescence, Gilet *et al.*[19] reported that the evolution of the vortices inside the drop may help the interface pinch-off and the formation of a secondary droplet. The contour plots of the vorticity $\omega_z(s^{-1})$ are presented in Figs. 11 and 12 for eight different time steps after the film rupture. As before, the solid lines represent the drop and bulk fluid interface while the dashed lines at the bottom delineate the area of the tracer particles. The evolution of the vortices inside the droplet for $\varphi = 0$ is presented in Fig. 11. Two counter-rotating vortices are observed at the bottom of the drop immediately after the film rupture, with intensities that

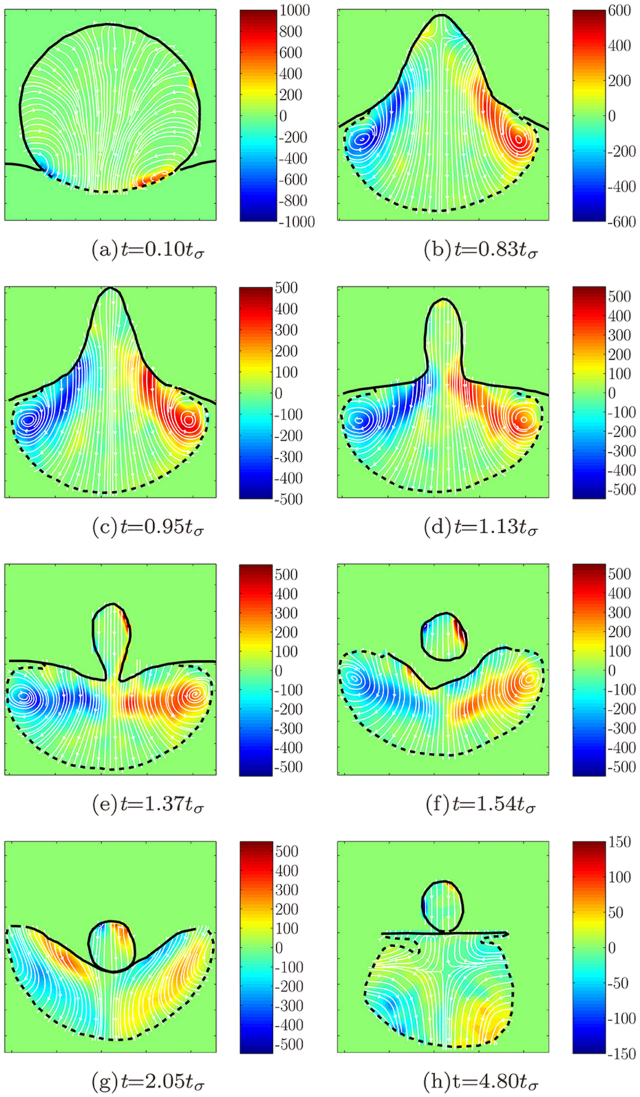

FIG. 11. Time-resolved streamlines and contour plots of vorticity ω_z for $\varphi = 0$.

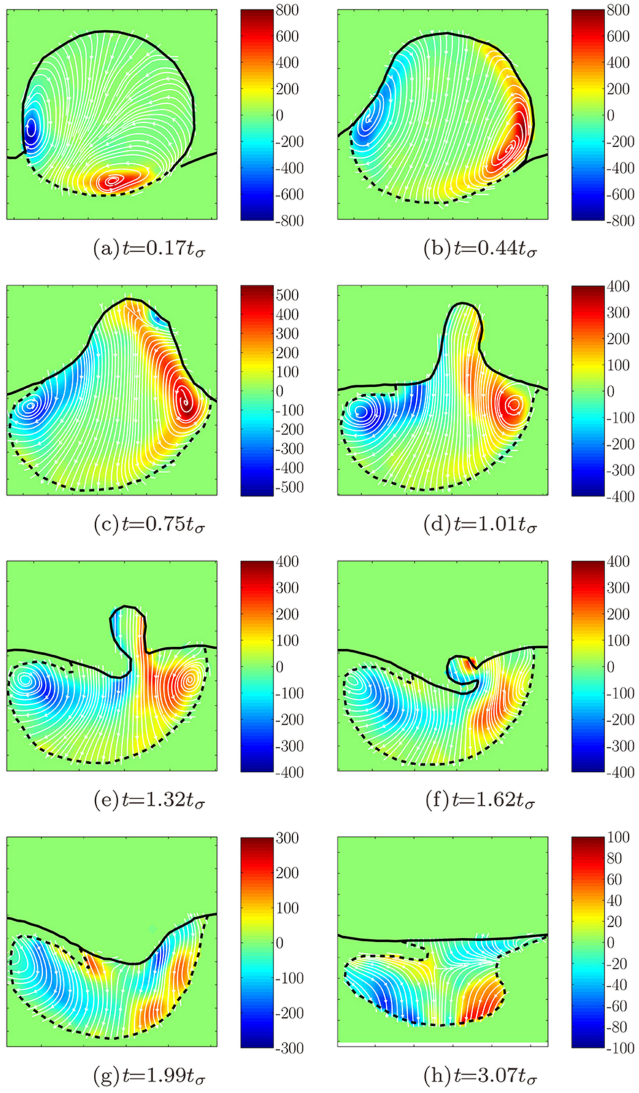

FIG. 12. Time-resolved streamlines and contour plots of vorticity ω_z for $\varphi = 1.3 \times 10^{-6}$.

are similar in magnitude and absolute vorticity levels varying in the range $|\omega_z| = 0\text{-}750\ \text{s}^{-1}$.

Until $t = 0.83t_\sigma$, the cores of the vortices move outwards and upwards along with the edges of the neck in a symmetrical way. As the edges continue to retract, the top of the drop acquires a conical shape and the peak value of $|\omega_z|$ decreases to 450 s^{-1} at $t = 0.83t_\sigma$. At the same time, the vortical structures acquire a tadpole shape. Two tail areas with high $|\omega_z|$ are observed connected to the cores of the vortices. As the flow changes from a horizontal to a downward direction in the tail area, the vorticity reaches a value of $|\omega_z| = 550\ \text{s}^{-1}$, larger than that in the core of the vortices ($|\omega_z| = 330\ \text{s}^{-1}$). From $t = 0.83t_\sigma$ to $t = 1.37t_\sigma$, the edges of the neck converge and lead to pinch-off, the high vorticity tail areas are pushed downwards and the cores of the vortices continue to move outwards in the bulk phase. ω_z of the tail area is decreased to $350\ \text{s}^{-1}$ at $t = 1.37t_\sigma$. After the pinch-off, the highly curved interface tends to return to the flat level under the effect of surface tension, while the liquid beneath the interface continues to move downwards due to inertial effects. Symmetrical vortices form beneath the interface from $t = 1.54t_\sigma$ to $t = 2.05t_\sigma$. Eventually the vortices move towards the centre and their strength diminishes. In partial coalescence, the vortices do not enter the liquid cylinder region and just remain below the interface. It can therefore be assumed that the vortices do not affect both the formation of the liquid cylinder and the pinch-off.

The evolution of vorticity for $\varphi = 1.3 \times 10^{-6}$ is presented in Fig. 12. At the early stages, two counter-rotating vortices are created at the bottom of the droplet near the edges of the neck with absolute values of $|\omega_z|$ up to $700\ \text{s}^{-1}$. At $t = 0.17t_\sigma$, the core of the left vortex has moved above the edge of the neck while the core of the right vortex is still below the edge. The intensity of the right vortex has slightly increased driven by the draining film. The downward motion in the central part of the drop increases the area occupied by the vortices and elongates them. Two long tails with high ω_z are created as a result of the changing flow direction from horizontal to vertical at $t = 0.75t_\sigma$. Contrary to $\varphi = 0$, the vorticity tails are able to reach the top part of the droplet in this case. The core of

the left vortex is below the neck edge and its tail becomes suppressed when the interface moves inwards at t = $1.01t_\sigma$. At the same time, the tail of the right vortex is also dampened by the inward motion of the drop surface on the right side. A liquid cylinder is formed at $t = 1.32t_\sigma$ and two asymmetric vortical areas are observed below the cylinder. From $t = 1.32t_\sigma$ to $t = 1.99t_\sigma$, the locations of the two cores are less affected by the irregular motion of the interface and they do not change location until the interface becomes smooth. When the surfactant concentration increases to $\varphi = 1.3 \times 10^{-4}$, total coalescence is observed and the evolution of the vortices was discussed in a previous study by Weheliye, Dong, and Angeli.[29]

IV. CONCLUSIONS

The partial coalescence of an aqueous drop with an organic-aqueous interface and the effect of surfactants were studied experimentally. The evolution of the interface shape and the velocity fields inside the drop were investigated with shadowgraphy and with high speed PIV, respectively. A critical Oh_c number is found for the partial coalescence for small Bo. When surfactants are introduced into the organic phase, the partial coalescence region in the Oh–Bo map is found to reduce. In addition, the drop size ratio, ξ, of the daughter to mother drop size, decreased in the inertio-capillary regime with increasing surfactant concentration. As the daughter droplet is considered to have higher concentration of surfactants on its surface than the mother droplet,[2] the drop ratio reduces at the later stages of the partial coalescence.

While the rupture of the film, which separates the drop from the interface, occurs close to the central vertical axis when there are no surfactants, in the presence of surfactants, the rupture occurs off-axis. After rupture and at the early stages of coalescence, the inward movement of the liquid in the upper part of the drop creates a liquid cylinder. The strong downward flow of the fluid inside the droplet creates a low-pressure area at the bottom of the liquid cylinder in the subsequent stages. In a system without surfactants, this low pressure aids the pinch-off of a daughter drop and leads to partial coalescence. However, in the presence of surfactants, the liquid cylinder is not symmetric and does not pinch off. It is also found that vortices developing inside the droplet do not have a significant effect on partial coalescence.

Partial coalescence may be affected by the size and the structure of the surfactants. Further studies of the velocity fields during coalescence with different types of surfactants are therefore needed. These should be complemented by investigation of the changes in pressure inside the drop to further elucidate the partial coalescence mechanism. In addition, the distribution of surfactants along the interface during drop coalescence has only been obtained from numerical simulations. Experimental work in this area is therefore needed.

ACKNOWLEDGMENTS

This project was funded by the UK Engineering and Physical Sciences Research Council (EPSRC) Programme Grant MEMPHIS. The authors would like to acknowledge the EPSRC Instrument Pool for the loan of the high-speed camera. Teng Dong would also like to thank the Chinese Scholarship Council (CSC) for providing his studentship.

[1] E. X. Berry and R. L. Reinhardt, "An analysis of cloud drop growth by collection: Part I. Double distributions," J. Atmos. Sci. **31**, 1814–1824 (1974).
[2] D. W. Martin and F. Blanchette, "Simulations of surfactant effects on the dynamics of coalescing drops and bubbles," Phys. Fluids **27**, 012103 (2015).
[3] F. Raes, R. Van Dingenen, E. Vignati, J. Wilson, J.-P. Putaud, J. H. Seinfeld, and P. Adams, "Formation and cycling of aerosols in the global troposphere," Atmos. Environ. **34**, 4215–4240 (2000).
[4] W. Rommel, E. Blass, and W. Meon, "Plate separators for dispersed liquid—liquid systems: The role of partial coalescence," Chem. Eng. Sci. **48**, 1735–1743 (1993).
[5] J. Benjamins, M. H. Vingerhoeds, F. D. Zoet, E. H. De Hoog, and G. A. Van Aken, "Partial coalescence as a tool to control sensory perception of emulsions," Food Hydrocolloids **23**, 102–115 (2009).
[6] L. Mahajan, "Liquid drops on the same liquid surface," Nature **126**, 761–767 (1930).
[7] G. E. Charles and S. G. Mason, "The mechanism of partial coalescence of liquid drops at liquid/liquid interfaces," J. Colloid Sci. **15**, 105–122 (1960).
[8] F. Blanchette and T. P. Bigioni, "Partial coalescence of drops at liquid interfaces," Nat. Phys. **2**, 254–257 (2006).
[9] B. Ray, G. Biswas, and A. Sharma, "Generation of secondary droplets in coalescence of a drop at a liquid-liquid interface," J. Fluid Mech. **655**, 72 (2010).
[10] P. Pikhitsa and A. Tsargorodskaya, "Possible mechanism for multistage coalescence of a floating droplet on the air/liquid interface," Colloids Surf., A **167**, 287–291 (2000).
[11] G. Pucci, D. Harris, and J. Bush, "Partial coalescence of soap bubbles," Phys. Fluids **27**, 061704 (2015).
[12] F. Blanchette, L. Messio, and J. W. Bush, "The influence of surface tension gradients on drop coalescence," Phys. Fluids **21**, 072107 (2009).
[13] P. Yue, C. Zhou, and J. J. Feng, "A computational study of the coalescence between a drop and an interface in newtonian and viscoelastic fluids," Phys. Fluids **18**, 102102 (2006).
[14] F. Zhang, E. Li, and S. T. Thoroddsen, "Satellite formation during coalescence of unequal size drops," Phys. Rev. Lett. **102**, 104502 (2009).
[15] A. Mar and S. Mason, "Coalescence in three-phase fluid systems," Colloid Polym. Sci. **224**, 161–172 (1968).
[16] A. D. Nikolov, D. T. Wasan *et al.*, "Effects of surfactant on multiple stepwise coalescence of single drops at liquid-liquid interfaces," Ind. Eng. Chem. Res. **34**, 3653–3661 (1995).
[17] X. Chen, S. Mandre, and J. J. Feng, "Partial coalescence between a drop and a liquid-liquid interface," Phys. Fluids **18**, 051705 (2006).
[18] C. Kinoshita, H. Teng, and S. Masutani, "A study of the instability of liquid jets and comparison with Tomotika's analysis," Int. J. Multiphase Flow **20**, 523–533 (1994).
[19] T. Gilet, K. Mulleners, J.-P. Lecomte, N. Vandewalle, and S. Dorbolo, "Critical parameters for the partial coalescence of a droplet," Phys. Rev. E **75**, 036303 (2007).
[20] Z. Mohamed-Kassim and E. K. Longmire, "Drop coalescence through a liquid/liquid interface," Phys. Fluids **16**, 2170–2181 (2004).
[21] S. Tomotika, "On the instability of a cylindrical thread of a viscous liquid surrounded by another viscous fluid," Proc. R. Soc. London, Ser. A **150**, 322–337 (1935).
[22] H. P. Kavehpour, "Coalescence of drops," Annu. Rev. Fluid Mech. **47**, 245–268 (2015).
[23] B. Dai and L. G. Leal, "The mechanism of surfactant effects on drop coalescence," Phys. Fluids **20**, 040802 (2008).
[24] T. Hodgson and J. Lee, "The effect of surfactants on the coalescence of a drop at an interface I," J. Colloid Interface Sci. **30**, 94–108 (1969).
[25] Y. Yoon, A. Hsu, and L. G. Leal, "Experimental investigation of the effects of copolymer surfactants on flow-induced coalescence of drops," Phys. Fluids **19**, 023102 (2007).
[26] L. Y. Yeo, O. K. Matar, E. S. P. de Ortiz, and G. F. Hewitt, "Film drainage between two surfactant-coated drops colliding at constant approach velocity," J. Colloid Interface Sci. **257**, 93–107 (2003).
[27] J. Lu and C. M. Corvalan, "Coalescence of viscous drops with surfactants," Chem. Eng. Sci. **78**, 9–13 (2012).

[28]M. Benmekhbi, S. Simon, and J. Sjöblom, "Dynamic and rheological properties of span 80 at liquid–liquid interfaces," J. Dispersion Sci. Technol. **35**, 765–776 (2014).
[29]W. H. Weheliye, T. Dong, and P. Angeli, "On the effect of surfactants on drop coalescence at liquid/liquid interfaces," Chem. Eng. Sci. **161**, 215–227 (2017).
[30]W. Weheliye, M. Yianneskis, and A. Ducci, "On the fluid dynamics of shaken bioreactors-flow characterization and transition," AIChE J. **59**, 334–344 (2013).
[31]A. Ducci and W. H. Weheliye, "Orbitally shaken bioreactors-viscosity effects on flow characteristics," AIChE J. **60**, 3951–3968 (2014).
[32]S. Thoroddsen and K. Takehara, "The coalescence cascade of a drop," Phys. Fluids **12**, 1265–1267 (2000).
[33]F. Zhang, M.-J. Thoraval, S. T. Thoroddsen, and P. Taborek, "Partial coalescence from bubbles to drops," J. Fluid Mech. **782**, 209–239 (2015).
[34]D. W. Fallest, A. M. Lichtenberger, C. J. Fox, and K. E. Daniels, "Fluorescent visualization of a spreading surfactant," New J. Phys. **12**, 073029 (2010).
[35]H. Ding, E. Li, F. Zhang, Y. Sui, P. D. Spelt, and S. T. Thoroddsen, "Propagation of capillary waves and ejection of small droplets in rapid droplet spreading," J. Fluid Mech. **697**, 92–114 (2012).